Laminar Burning Velocities and Markstein Numbers of Hydrocarbon / Air Flames

L.-K. TSENG, M. A. ISMAIL, and G. M. FAETH*
Department of Aerospace Engineering, The University of Michigan, Ann Arbor, MI 48109-2140

Effects of positive flame stretch on the laminar burning velocities of hydrocarbon/air mixtures were studied experimentally using outwardly propagating spherical flames. The test conditions included propane, methane, ethane, and ethylene–air flames at various fuel-equivalence ratios and normal temperature and pressure. Karlovitz numbers generally were less than 0.3 so that the flames were remote from quenching conditions. Within this range, the ratio of the unstretched (plane flames) to stretched laminar burning velocities varied linearly with Karlovitz numbers, yielding Markstein numbers that were independent of Karlovitz numbers for a particular reactant mixture. In addition, Markstein numbers varied in a roughly linear manner with fuel-equivalence ratios over the range of the measurements, which were somewhat removed from flammability limits where behavior might differ. Effects of stretch were substantial: Markstein numbers varied from −2.5 to 7.2, yielding corresponding laminar burning velocity variations of 0.4–2.7 times the value for an unstretched (plane) flame over the test range. The ranges of fuel-equivalence ratios for unstable preferential-diffusion conditions (negative Markstein numbers) were as follows: propane, greater than 1.44; methane, less than 0.74; ethane, greater than 1.68; and ethylene, greater than 1.95. Fuel-equivalence ratios for maximum flame temperatures and laminar burning velocities are near unity for the present flames; therefore, neutral preferential-diffusion conditions are shifted toward fuel-equivalence ratios on the unstable side of unity, in qualitative agreement with recent approximate theories treating the effects of stretch on laminar premixed flames.

NOMENCLATURE

D	mass diffusivity
K	flame stretch
Ka	Karlovitz number, $K D_u/S_L^2$
L	Markstein length, Eq. 1
Ma	Markstein number, L/δ_D
r_f	flame radius
S	sensitivity of Ma to ϕ, Eq. 10
S_L	laminar burning velocity based on unburned gas properties
$S'_{L\infty}$	value of S_L at largest radius observed
t	time
δ_D	characteristic flame thickness, D_u/S_L
$\Delta(dr_f/dt)$	velocity difference between cold and hot flame boundaries
$\Delta(S_L)$	difference of S_L found relative to the velocities of the cold and hot flame boundaries
ρ	density
ϕ	fuel-equivalence ratio
ϕ_n	ϕ at neutral stability condition

Subscripts

b	burned gas properties
max	maximum observed value
u	unburned gas properties
∞	asymptotic condition for an unstretched (plane) flame

INTRODUCTION

Recent measurements have shown that effects of flame stretch on laminar burning velocities significantly affect the properties of strongly turbulent premixed flames in the thin-flamelet regime, and suggest that these effects are important for most practical premixed turbulent flames [1]. The mechanism responsible for this behavior involves interactions between the preferential-diffusion of various species and heat, and the distortion of the flame surface by turbulence; this causes turbulent distortion of

* Corresponding author: G. M. Faeth 218 Aerospace Engineering Building, The University of Michigan, Ann Arbor, MI 48109-2140.

0010-2180/93/$6.00

the flame surface to be either retarded or enhanced for stable or unstable preferential-diffusion conditions, respectively. Thus, recent experimental evaluations of numerical simulations of turbulent premixed flames have been limited to neutral preferential-diffusion conditions, where laminar burning velocities are independent of stretch, so that this complication can be avoided [2, 3]. In order to provide information needed to move beyond the singular neutral preferential-diffusion condition, the objective of the present investigation was to experimentally study the effects of stretch on propane, methane, ethane, and ethylene/air flames. The approach involved observations of outwardly propagating spherical laminar flames using methods recently developed during a study of $H_2/O_2/N_2$ flames [4]. The work also involved reanalysis of existing measurements of flame radius as a function of time for the same flame configuration and fuels [5–9], for comparison with the present results.

Freely propagating flames involve effects of finite flame thickness, curvature, and unsteadiness that must be considered in order to properly define laminar burning velocities and flame stretch. These difficulties will be discussed later; however, they will be ignored for the present in order to introduce concepts used during this study in a relatively simple manner. This implies limiting considerations to thin flames, having a large radius of curvature, with slowly varying flame stretch so that effects of curvature and unsteadiness can be neglected. For these conditions, the relationship between the laminar burning velocity and flame stretch is normally written according to an early proposal of Markstein [10] as follows [7–16]:

$$S_L = S_{L\infty} - LK, \tag{1}$$

where S_L is the rate of propagation of the flame relative to the unburned gas, and $S_{L\infty}$ is the value of S_L for an unstretched (plane) flame ($K = 0$). The coefficient L is a measure of the response of the flame to stretch, called the Markstein length [11]. Naturally, it is an important issue to gain an understanding of the factors that can influence the value of the Markstein length, for example, effects of the properties of the reactant mixture, effects of the flame stretch itself (analogous to effects of driving potentials on transport coefficients), and effects of the flame configuration (steady or unsteady, adiabatic or quenched by radiation or surfaces, etc.), among others. Kwon et al. [4] make the assumption (or local conditions hypothesis) that the Markstein length is proportional to the local characteristic flame thickness, δ_D, because both are representative of the scale of distances over which the diffusion of mass and heat occurs in flames. Thus, a dimensionless Markstein number, is defined as follows:

$$\mathrm{Ma} = L/\delta_D \tag{2}$$

The corresponding dimensionless parameter to describe flame stretch was taken to be the Karlovitz number, also based on local flame conditions [4], which is the ratio of the local characteristic flame residence time, δ_D/S_L, and the characteristic flame stretch time, K^{-1}, or [15, 16]:

$$\mathrm{Ka} = K\delta_D/S_L. \tag{3}$$

Then substituting Eqs. 2 and 3 into Eq. 1, and rearranging, yields the following dimensionless relationship between the laminar burning velocity and stretch:

$$S_{L\infty}/S_L = 1 + \mathrm{Ma}\,\mathrm{Ka}. \tag{4}$$

Finally, the definitions of Ma and Ka in Eqs. 2–4 are completed by specifying the characteristic flame thickness. This choice is somewhat arbitrary because the thickness can be based on relative velocities at various points and any one of several mass diffusivities of the reactant species or the thermal diffusivity [11], all of which vary significantly within the flame. However, a convenient choice for reducing experimental data and for scaling purposes is to base δ_D on the laminar burning velocity and the mass diffusivity of the fuel in the unburned gas, as follows [4]:

$$\delta_D = D_u/S_L. \tag{5}$$

Most practical flame systems are highly diluted (e.g., combustion in air) so that D_u can be taken as the binary diffusivity of the fuel with respect to the diluent in order to approximate

its diffusion properties in the reactant mixture with little error [4]—a practice that will be adopted in the following.

The main issues with respect to fundamental laminar burning velocities, effects of stretch on laminar burning velocities, and numerical simulations of turbulent flames, are the values of $S_{L\infty}$ and Ma, and how Ma varies with the factors enumerated earlier [1–4]. Experiments to determine these properties have been based on outwardly propagating spherical flames, steady flames in stagnation flows and buoyant jet flames [4–27]. Strehlow and Savage [17], however, point out the advantages of outwardly propagating spherical flames because both S_L and Ka can be found in a simple and straight forward manner. For example, assuming a spherical laminar deflagration wave propagating away from an ignition source, negligible motion of the burned gas, and negligible curvature and transient effects associated with the thickness of the flame (which implies $\delta_D/r_f \ll 1$ as a necessary condition), the laminar burning velocity is given by [17]

$$S_L = (\rho_b/\rho_u)dr_f/dt, \tag{6}$$

with a corresponding expression for K as follows:

$$K = (2/r_f)dr_f/dt. \tag{7}$$

Thus, when the present assumptions are satisfied, Eqs. 6 and 7 readily yield S_L and K from observations of r_f as a function of time, for example, using shadowgraph or schlieren techniques with adequate definition of r_f assured because $\delta_D/r_f \ll 1$.

Effects of flame thickness, curvature and unsteadiness, ignored until now, complicate measurements of S_L and K using outwardly propagating spherical flames in conjunction with Eqs. 6 and 7, as well as the interpretation of effects of flame stretch on laminar burning velocities [11]. Effects of flame thickness and curvature on such determinations of S_L have been recognized for some time [27]. The main difficulties involve changes of flame structure when evolving from nearly spherically symmetric flames at small r_f to nearly plane flames at large r_f, effects of variations of cross-sectional area on velocities within the flames, and variations of the position of the flame that is indicated by shadowgraph and schlieren techniques, relative to the hot and cold flame boundaries, as changing effects of curvature modify the flame structure. Nevertheless, these problems can be avoided by limiting measurements to conditions where $\delta_D/r_f \ll 1$ [27], which was the approach used during the present investigation.

Effects of unsteadiness on the interpretation of measurements of outwardly propagating spherical flames were recognized more recently by Sivashinsky and coworkers [28, 29], among others [11]. These effects are caused by variations of S_L due to changes of K with r_f, as indicated by Eqs. 1, 6, and 7. This implies corresponding changes of flame thickness through Eq. 5, so that the hot and cold boundaries of the flame no longer move at the same velocity, somewhat analogous to effects of flame curvature. This leads to an uncertainty of dr_f/dt, with corresponding uncertainties of S_L, K, and L, as suggested by Eqs. 1, 6, and 7. Clavin [11] describes effects of unsteadiness by defining two laminar burning velocities, relative to the motion of the hot and cold flame boundaries, respectively, along with two Markstein lengths corresponding to these velocities. Instead of applying this formulation, which involves adopting a particular simplified model of flame structure, however, the present study was limited to conditions where effects of unsteadiness were small. The required experimental conditions can be identified by finding the difference between the velocities of the hot and cold flame boundaries, $\Delta(dr_f/dt)$. This difference also is proportional to the difference between the laminar burning velocities found relative to the motion of the hot and cold flame boundaries, $\Delta(S_L)$, through Eq. 6, at least for conditions where $\Delta(dr_f/dt)/(dr_f/dt)$ is small. Straightforward analysis of the motion of the hot and cold boundaries, assuming that effects of flame curvature are small, then yields the following relationships:

$$\begin{aligned}\Delta(dr_f/dt)/(dr_f/dt) &= \Delta(S_L)/S_L = d\delta_D/dr_f \\ &= -(\delta_D/S_L)dS_L/dr_f.\end{aligned} \tag{8}$$

Based on Eq. 8, as discussed later, effects of unsteadiness tend to be small when $\delta_D/r_f \ll 1$, and can be controlled in the same manner as effects of finite flame thickness and curvature.

Equation 7 indicates that effects of flame stretch for outwardly propagating spherical flames can best be observed when r_f is small. However, controlling ignition disturbances and satisfying the limitation that $\delta_D/r_f \ll 1$, generally precludes operation near extinction conditions [4], for example, maximum values of Ka tend to be less than 0.4 rather than the values near unity that correspond to near-extinction conditions [15]. Fortunately, values of Ma tend to be large so that significant effects of stretch still can be observed for relatively small values of Ka [4].

Another concern about the use of the outwardly propagating spherical flames to study effects of stretch on laminar burning velocities involves potential transition to unstable flames with wrinkled flame surfaces—precluding observations of spherical laminar flames in some instances. The relationship between preferential-diffusion/stretch interactions and the stability of thin flames is easily seen from Eqs. 4 and 7. If the Markstein number is negative, the laminar burning velocity increases as the flame stretch (or Ka) increases through Eq. 4: then bulges due to disturbances in a nearly plane flame surface that are concave (convex) toward the combustion products have positive (negative) stretch (Ka), analogous to Eq. 7 for spherical flames; thus, the bulges grow and the flame is unstable. Conversely, if the Markstein number is positive, the laminar burning velocity decreases with increasing stretch (Ka), and similar bulges in the flame surface become smaller so that the flame is stable to preferential-diffusion effects. However, even outwardly propagating spherical flames that are stable to preferential-diffusion effects are subject to hydrodynamic instability because they involve the acceleration of a low-density gas toward a high-density gas [10, 11]. Fortunately, both observations [4, 26], and theory [30], show that transition to unstable flames from both preferential-diffusion and hydrodynamic instabilities for outwardly propagating spherical flames generally is sufficiently deferred so that preferential-diffusion/stretch interactions can be studied even when Markstein numbers are negative [4]. Thus, all things considered, measurements of outwardly propagating spherical flames, interpreted using Eqs. 1–7 for $\delta_D/r_f \ll 1$, provide a simple, direct, and relatively flexible approach to study effects of flame stretch on laminar burning velocities, as advocated by Strehlow and Savage [17].

Several studies of the effects of stretch on laminar burning velocities based on measurements of outwardly propagating spherical flames have been reported [4–9]. The measurements of $S_{L\infty}/S_L$ for $H_2/O_2/N_2$ and propane/air flames of Refs. 4–6 have been treated using Eqs. 1–7, finding a linear variation with Ka for each reactant mixture over the test range (Ka < 0.36) [4]: this implies Ma only depends the fuel-equivalence ratio. Even though quenching conditions were not approached, the effect of stretch on laminar burning velocities was substantial: Ma varied in the range -3 to 13 with corresponding variations of $S_{L\infty}/S_L$ of 0.5 to 3.1 for the two fuels. Thus, large values of Ma are not confined to fuels having unusually large mass diffusivities like hydrogen, relative to the mass diffusivities of other major species and the thermal diffusivity of the mixture. This helps explain recent observations of significant effects of stretch on strongly turbulent flames in both $H_2/O_2/N_2$ and hydrocarbon/air mixtures, see the discussion in Wu et al. [1]. The large values of Ma also raise questions about the available data base for laminar burning velocities in spite of past efforts to minimize stretch, because existing measurements involve finite, and generally unknown, values of Ka. Thus, values of the fundamental laminar burning velocity, $S_{L\infty}$, found from the measurements of Palm-Leis and Strehlow [5] for propane/air mixtures, were shifted from other measurements in the literature [18–24]—raising questions about whether this was an effect of stretch or a problem with their data [4].

Several other experimental investigations of the effects of stretch on laminar burning velocities have been reported using a variety of methods [7–9, 12–14]. The main difficulty with these studies is that simplified asymptotic theories were used to interpret the measurements, which introduces uncertainties due to the approximations of the theories that are difficult

to quantify. In particular, values of Ma and L for $H_2/O_2/N_2$ and propane/air mixtures using the direct approach of Eqs. 1–7 [4], and the approximate one-step global theories [7–9, 12, 14], are not in qualitative agreement—including the crucial determination of the neutral preferential-diffusion stability condition. Additionally, Searby and Quinard [14] show that flames stabilized in stagnating flows [12, 13] involve unacceptably large uncertainties of S_L and Ka from flow structure measurements. Finally, an alternative downward propagating flame technique used by Searby and Quinard [14] involves interactions between stabilizing Rayleigh–Taylor effects and preferential-diffusion instabilities which complicate the interpretation of their measurements.

To summarize, a recent study of the effects of stretch on laminar burning velocities has demonstrated the value of direct analysis (Eqs. 1–7) of experiments for outwardly propagating spherical flames, and has raised questions about the existing data base for laminar burning velocities and Markstein numbers for hydrocarbon/air flames [4]. Thus, the objectives of the present investigation were to use the approach of Ref. 4 to study these issues for typical hydrocarbon/air flames at normal temperature and pressure. Propane, methane, ethane, and ethylene/air flames were considered in order to provide a range of mass diffusion properties of the fuel. The study involved both new measurements, as well as reanalysis of existing measurements of flame radius as a function of time for outwardly propagating spherical flames from Refs. 5, 6, and 9.

The article begins with a description of experimental methods. This is followed by a discussion of the results, considering the general behavior of the flames, fundamental laminar burning velocities of plane flames, burning velocity/stretch interactions, and Markstein numbers, in turn.

EXPERIMENTAL METHODS

Apparatus

The present experiments were carried out in a windowed test chamber developed by Groff [26] that also was used for earlier premixed flame studies in this laboratory [1–4]. The chamber is quasi-spherical with a volume of 0.011 m^3 and a 260-mm cross-sectional diameter at its center. Optical access is provided by two 92-mm-diameter quartz windows mounted opposite one another in the end caps of the chamber.

The combustible mixture was prepared within the chamber by adding fuel and air at appropriate partial pressures to reach an initial pressure of 1 atm for all tests. The gases were mixed using fans within the chamber and then allowed to become quiescent prior to ignition. After combustion was complete, the chamber was vented and purged with dry air to remove condensed water vapor, prior to evacuating and refilling the chamber for the next test.

The spark ignition system was the same as Ref. 4. This involved electrodes extending from the top and bottom of the chamber, one fixed and the other positioned with an accuracy of 10 μm using a micrometer. The tips of the electrodes were 250-μm-diameter tungsten wires with a free length of 25 mm and a spark gap of 500 μm. The spark energy was supplied by a high-voltage capacitor circuit having a variable capacitance (100–5000 pF) and voltage (3–5 kV), and a discharge time of roughly 5 μs. Spark energies were adjusted by trial so that they were close to minimum ignition energies for the present spark gap, in order to minimize effects of spark disturbances. This involved stored spark energies in the range 10–200 mJ, tending to progressively increase with increasing preferential-diffusion stability (increasing Ma) of the reactant mixture.

Instrumentation

The flames were observed using shadowgraph motion picture photography, similar to Ref. 4. The shadowgraph system was based on a 100-W mercury lamp (ARC, HSA-150 HP), with the light collimated by a pair of $f6$ parabolic reflectors having focal lengths of 1220 mm. The shadowgraphs were recorded using a 16-mm motion picture camera (Hycam, Model K20 S4E) operating at 3000 pictures per second with a 1/10 shutter to yield an exposure time of 35 μs. Kodak Plus X film was used for the photographs. The framing rate of the camera

was sensed electronically so that ignition only occurred when the proper framing rate was reached. The framing rate and the ignition pulse were recorded using a digital oscilloscope (LeCroy 9400 A) so that the film records could be synchronized.

The films were measured by projecting them using an overall magnification of 4:1. The flames were nearly spherical (maximum and minimum diameters were within 10% of the mean diameter) but were measured horizontally to avoid the disturbances of the spark electrodes in the vertical direction. The overall resolution of the flame diameter measurements generally was less than 150 μm.

Data Reduction

Measurements of laminar burning velocities were limited to relatively small flames having diameters less than 60 mm. Within this region, the volume of burned gas was less than 1% of the total chamber volume and pressure transducer records showed that the chamber pressure was constant within 2%. Laser velocimeter measurements indicated that velocities within the unburned gas corresponded to the behavior expected for unconfined freely propagating spherical flames [2].

Potential effects of flame thickness and curvature were controlled by limiting δ_D/r_f to values less than 0.02 for the conditions where measurements were made. These same conditions also controlled effects of unsteadiness. In particular, velocity differences between the cold and hot flame boundaries were largest for propane/air flames at $\phi = 0.8$, where values of S_L were relatively low while dS_L/dr_f was relatively large due to strong effects of stretch. At this worst-case condition, however, $\Delta(dr_f/dt)/(dr_f/dt) = \Delta(S_L)/S_L$ was still less than 2% from Eq. 8, while finding δ_D based on cold boundary transport properties from Eq. 5. Even taking a more conservative approach, and using larger values of δ_D based on hot boundary conditions, as discussed later, still yielded uncertainties of dr_f/dt and S_L less than 7%. These uncertainties were smaller at other test conditions and generally were negligible in comparison to present experimental uncertainties; therefore, Eqs. 1–7 were used to interpret the measurements with no distinction made between the hot and cold flame boundary reference frames. Formally, however, present results correspond to use of the hot flame boundary reference frame defined by Clavin [11].

Rates of radiative heat loss were less than 1% of the rate of chemical energy release within the test flames, based on computations assuming adiabatic flame conditions throughout the burned gas region [31]. Thus, S_L was found from Eq. 6, assuming constant pressure adiabatic combustion with the reactant gas temperature equal to the initial temperature and negligible motion of the burned gas. The density ratio needed in Eq. 6 was found assuming thermodynamic equilibrium in the combustion products for adiabatic constant-pressure combustion using the Gordon and McBride [32] algorithm. Similar to Ref. 4, the corresponding values of the Karlovitz number were found by eliminating δ_D between Eqs. 3 and 5 to yield

$$\mathrm{Ka} = KD_u/S_L^2 \tag{9}$$

with K being found from Eq. 7. The values of dr_f/dt needed to find S_L and Ka were obtained using local polynomial fits of the measurements of r_f as a function of time, averaging the results of four tests at each condition. The mass diffusivity appearing in Eq. 9 was taken to be that of the fuel in nitrogen at unburned gas conditions, found from Ref. 33.

Experimental uncertainties (95% confidence) of dr_f/dt and S_L were less than 5 and 15%, respectively. The higher uncertainty of S_L reflects estimated uncertainties of the density ratio in Eq. 6 and potential effects of the slight chamber pressure increase, unsteadiness and radiative heat losses from the burned gas [27]. The corresponding uncertainties of Ka from Eq. 9 generally were less than 25%.

The measurements of Palm-Leis and Strehlow [5], Fristrom [6], and Taylor [9] also were reduced by present methods, using their reported values of flame radius as a function of time (or S_L as a function of r_f). Estimates of experimental uncertainties are not reported for these studies. However, the results seem con-

sistent and probably have similar experimental uncertainties, aside from uncertainties due to transcribing data from plots and potential problems concerning the fuel-equivalence ratio values reported by Palm-Leis and Strehlow [5], as discussed in Ref. 4.

Test Conditions

Present test conditions for propane, methane, ethane, and ethylene/air flames are summarized in Table 1. Corresponding tables summarizing the Palm-Leis and Strehlow [5] and Fristrom [6] measurements appear in Ref. 4. The test conditions of Taylor [9] are similar to the present measurements; the original source should be consulted for details.

Table 1 is organized in terms of the fuel-equivalence ratio and provides the values of ρ_u/ρ_b and D_u used to reduce the data. Values of $S'_{L\infty}$ were found directly at the largest radius where measurements were made while values of $S_{L\infty}$ were found by extrapolating the data to $\mathrm{Ka} \rightarrow 0$, as discussed later. Differences between $S'_{L\infty}$ and $S_{L\infty}$ are representative of effects of stretch on conventional direct determinations of laminar burning velocities for normal laboratory conditions. These discrepancies tend to be largest at the smallest or largest fuel-equivalence ratio considered with maximum values for each fuel as follows: propane, 22% at $\phi = 1.8$; methane, 40% at $\phi = 0.6$; ethane, 4% at $\phi = 0.8$; and ethylene, 5% at $\phi = 0.8$. Thus, laminar burning velocities near

TABLE 1

Summary of Test Conditions[a]

ϕ (−)	ρ_u/ρ_b (−)	$S'_{L\infty}$ (mm/s)	$S_{L\infty}$ (mm/s)	$\delta_{D\infty}$ (μm)	$K_{\max}$ (s^{-1})	$\mathrm{Ka}_{\max}$ (−)	Ma (−)
Propane/Air (D_u = 11.3 mm^2/s)							
0.80	7.09	250	280	40	340	0.25	4.8
1.00	7.97	310	320	35	610	0.14	3.9
1.20	8.06	370	370	31	760	0.11	3.8
1.30	7.92	350	350	32	800	0.10	2.6
1.40	7.79	210	270	42	820	0.12	−0.2
1.60	7.52	160	140	80	580	0.15	−2.0
1.80	7.23	110	82	138	440	0.16	−2.5
Methane/Air (D_u = 21.9 mm^2/s)							
0.60	4.33	100	60	360	270	0.30	−1.9
0.70	4.77	180	180	120	450	0.30	−0.04
0.90	5.57	330	340	64	850	0.30	1.3
1.00	5.93	410	430	51	550	0.09	2.1
1.10	5.59	440	440	50	1010	0.20	1.9
1.20	5.23	430	440	50	860	0.23	2.6
1.35	4.69	340	390	56	240	0.23	7.2
Ethane/Air (D_u = 14.6 mm^2/s)							
0.80	6.00	260	270	54	400	0.20	1.6
1.00	6.87	380	400	37	810	0.25	2.1
1.10	6.69	440	450	32	1100	0.21	1.7
1.20	6.41	440	430	34	1260	0.21	1.1
1.40	5.70	320	330	44	750	0.19	0.6
1.60	5.29	205	200	73	470	0.21	−0.6
Ethylene/Air (D_u = 15.8 mm^2/s)							
0.80	7.83	360	380	42	750	0.18	2.7
0.90	8.26	440	460	34	820	0.09	2.0
1.00	8.59	540	580	27	1270	0.13	3.0
1.20	9.00	560	600	26	1510	0.11	2.5
1.30	9.11	540	560	28	1170	0.08	2.3
1.40	9.18	420	430	37	1210	0.14	1.1
1.60	9.24	280	290	54	910	0.22	0.5
1.80	9.26	170	170	93	380	0.24	0.2

[a] Initial mixture pressure and temperature 1 atm and 298 ± 3 K.

limits, particularly when the mass diffusivity of the fuel differs significantly from oxygen, are most affected by stretch and should be used with caution unless they have been corrected to $S_{L\infty}$. The characteristic flame thickness, $\delta_{D\infty}$, is found using $S_{L\infty}$ in Eq. 5, yielding the following ranges: propane, 31–138 μm; methane, 50–360 μm; ethane, 32–73 μm; and ethylene, 26–93 μm. Values of $\delta_{D\infty}$ based on burned gas conditions would be 2.8–4.3 times larger than the values listed in Table 1, yielding thicknesses of 120–1020 μm over the present test range. Maximum values of stretch were limited so that $\delta_D/r_f < 0.02$, yielding the following ranges: propane, 340–820 s^{-1}; methane, 240–1010 s^{-1}; ethane, 400–1260 s^{-1}; and ethylene, 380–1510 s^{-1}. It is easier to interpret relative effects of stretch using the maximum Karlovitz numbers, however, which have the following values: propane, 0.25; methane, 0.30; ethane, 0.25; and ethylene, 0.24. As mentioned earlier, these values are relatively small in comparison to the values on the order of unity that are associated with extinction conditions [15]; this is a natural consequence of avoiding measurements near the disturbances of spark kernels, while requiring δ_D/r_f and unsteady effects in the flames to be small. Values of Ma, found as described later, also are summarized in Table 1.

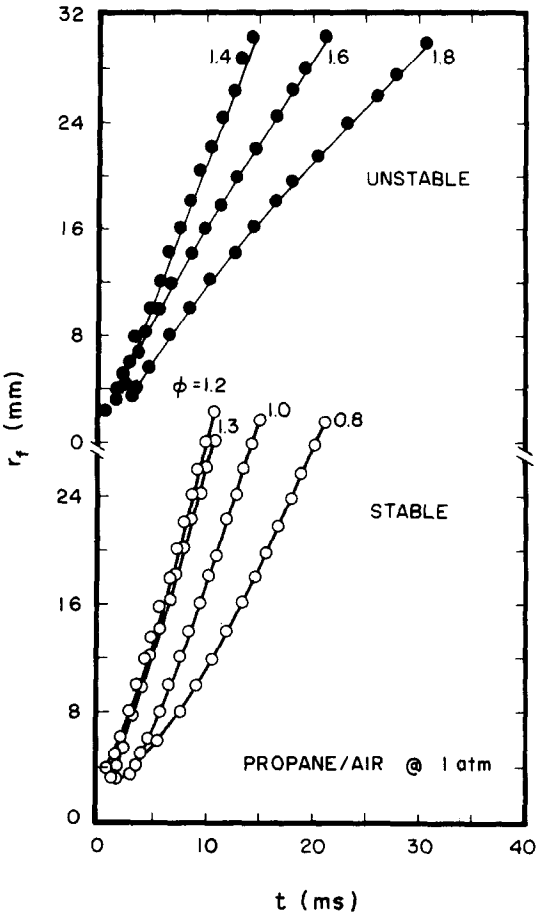

Fig. 1. Flame radius as a function of time for propane/air mixtures.

RESULTS AND DISCUSSION

Flame Evolution

Direct observations of flame radius as a function of time, and laminar burning velocity as a function of flame radius, will be considered first in order to indicate the nature of the measurements. Results for propane/air flames will be used for this purpose because they exhibit features observed for the other flames unusually well.

Flame radius as a function of time is plotted in Fig. 1 for all the fuel-equivalence ratios considered for the propane/air flames. Neutral and unstable preferential-diffusion conditions (Ma $\leq$ 0) are denoted by darkened symbols while stable preferential-diffusion conditions (Ma > 0) are denoted by open symbols; this practice will be adopted on all subsequent plots. Except for a very slow methane/air flame (ϕ = 0.6) that developed buoyant instabilities at a relatively small radius and is not considered here, all the present flames had smooth flame surfaces over the region where laminar burning velocity measurements were made, $r_f < 30$ mm. Flames for unstable preferential-diffusion conditions, however, developed irregular surfaces at larger radii. In contrast, the faster propagating $H_2/O_2/N_2$ flames exhibited relatively rapid transition to unstable flame surfaces for unstable preferential-diffusion conditions [4]. Effects of preferential-diffusion can be seen from the variation of the slopes of the plots in Fig. 1, which are proportional to S_L through Eq. 6. Thus, the slopes increase (decrease) with increasing r_f (or decreasing K through Eq. 7) for stable (unstable) conditions and tend toward constant values at

large r_f where the rate of change of K, and K itself, tends toward small values. Although no quantitative study of minimum ignition energies was made, a correspondence between minimum ignition energies and preferential-diffusion conditions was observed that has been noted by others [15]. This involved much smaller ignition energies for unstable than stable preferential-diffusion conditions, particularly as limits were approached. Thus, the preferential-diffusion mechanisms that cause S_L to increase at large K for unstable conditions, also appear to assist the ignition process.

The values of S_L for propane/air flames, for various flame radii corresponding to Fig. 1, are plotted in Fig. 2. (Note that results for $r_f < 5$ mm for $\phi = 0.8$ involve transient effects beyond the limits mentioned earlier and only are shown to exhibit general trends.) These results show that the effect of stretch on laminar burning velocities is substantial, particularly for conditions removed from the neutral stability condition, for example, at $\phi = 0.8$ and 1.8. It is surprising that this extraordinary behavior has received relatively little experimental attention even though Palm-Leis and Strehlow [5] reported similar findings more than 20 years ago. It also is evident that effects of stretch can persist to large flame radii, for example, see the results at $\phi = 0.8$. Due to the small values of δ_D/r_f for these flames (see Table 1), this behavior clearly is not a result of effects of the crosssectional area for transport within the thickness of the flame; rather, it is caused by flame stretch due to the outward propagation of the thin curved flame surface [17].

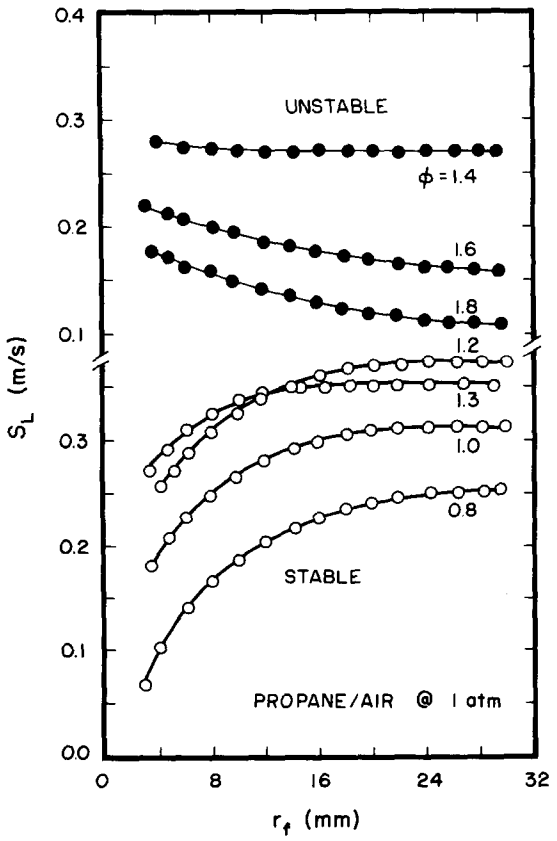

Fig. 2. Laminar burning velocity as a function of flame radius for propane/air mixtures.

Results for finite flame radii, like Fig. 2, involve finite values of K so that the values of the laminar burning velocities at the largest r_f observed, $S'_{L\infty}$, still differ from the fundamental laminar burning velocity for a plane flame, $S_{L\infty}$. Thus, values of $S_{L\infty}$ were found through Eq. 4 by plotting $S'_{L\infty}/S_L$ as a function of Ka. As subsequent results will show, these plots are linear so that extrapolation to Ka = 0 yields $S'_{L\infty}/S_{L\infty}$ and thus $S_{L\infty}$. This procedure was used to find the values of $S_{L\infty}$ and the corresponding values of $\delta_{D\infty}$, for the present measurements, summarized in Table 1, as well as for the other measurements for outwardly-propagating spherical flames [5, 6, 9]. This behavior highlights the advantage of the local conditions hypothesis which yields Ka directly from the measurements and provides a linear extrapolation to find $S_{L\infty}$; in contrast, if Ma and Ka are based on $S_{L\infty}$ values of Ka must be found iteratively and the extrapolation to find $S_{L\infty}$ no longer is linear.

Laminar Burning Velocities

The values of $S_{L\infty}$ found from the measurements of outwardly propagating spherical flames are plotted as a function of fuel-equivalence ratio for the four fuels in Figs. 3–6. Existing measurements in the literature, involving finite but generally unknown levels of flame stretch in spite of efforts to minimize stretch, also are shown on the plots [13, 18–25]. Andrews and Bradley [25] survey numerous

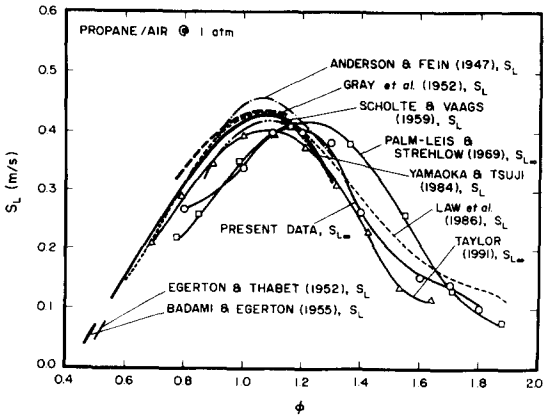

Fig. 3. Laminar burning velocity as a function of fuel-equivalence ratio for propane/air mixtures. Measurements of Palm-Leis and Strehlow [5], Taylor [9], Law et al. [13], Yamaoka and Tsuji [18], Scholte and Vaags [19], Anderson and Fein [20], Gray et al. [21], Harris et al. [22], Egerton and coworkers [23, 24], and the present study.

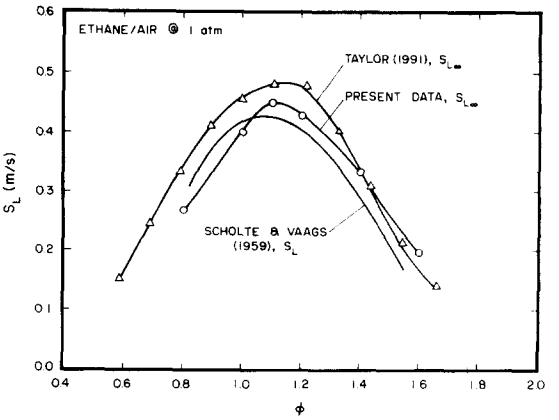

Fig. 5. Laminar burning velocity as a function of fuel-equivalence ratio for ethane/air mixtures. Measurements of Taylor [9], Scholte and Vaags [19], and the present study.

other early measurements of the laminar burning velocities of methane/air mixtures as well; however, only their results are shown as being representative of the others in order to avoid cluttering Fig. 4 excessively.

The first issue in connection with the laminar burning velocity measurements illustrated in Figs. 3–6 is the consistency of determinations of S_{L^x} from measurements of outwardly propagating spherical flames. Over all the fuels, present measurements and those of Taylor [9] generally agree within experimental uncertainties. However, results based on the measurements of Palm-Leis and Strehlow [5] for propane/air mixtures (Fig. 3) only yield comparable maximum values of S_{L^x} and clearly seem to be shifted toward larger fuel-equivalence ratios, indicating a problem with their reported values of fuel-equivalence ratios, as suggested in Ref. 4. Thus, only the results of Taylor [9] and the present measurements will be considered in the following comparisons between S_{L^x} found for outwardly propagating spherical flames and S_L reported using other methods.

In general, the various methods yield comparable maximum laminar burning velocities in Figs. 1–4 in view of anticipated experimental

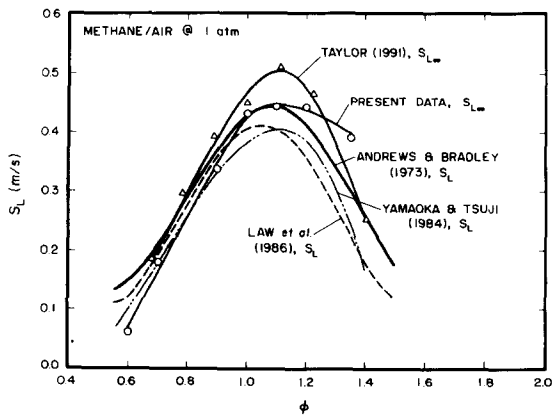

Fig. 4. Laminar burning velocity as a function of fuel-equivalence ratio for methane/air mixtures. Measurements of Taylor [9], Law et al. [13], Yamaoka and Tsuji [18], Andrews and Bradley [25], and the present study.

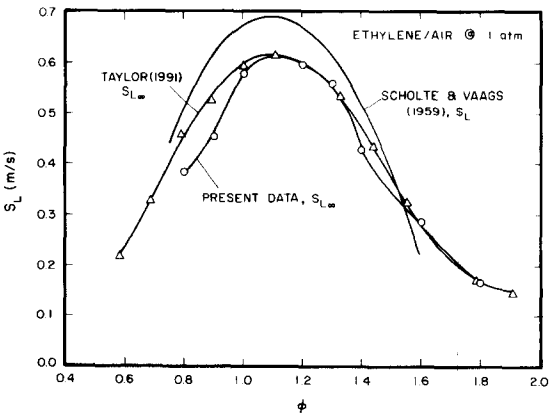

Fig. 6. Laminar burning velocity as a function of fuel-equivalence ratio for ethylene/air mixtures. Measurements of Taylor [9], Scholte and Vaags [19] and the present study.

uncertainties. The main difference between $S_{L\infty}$ and S_L is that $S_{L\infty}$ reaches a maximum near $\phi = 1.1-1.2$ while S_L reaches a maximum for $\phi = 1.0-1.1$, for all the fuels. This shift is systematic and might be significant; however, it only constitutes a 10% change, which is not large in comparison to the typical experimental uncertainties of concentration determinations. Finally, although values of S_L are limited to Scholte and Vaags [19] for ethane and ethylene/air flames (Figs. 5 and 6), $S_{L\infty}$ and S_L for these flames are in reasonably good agreement. This behavior is anticipated, however, because preferential-diffusion effects are weakest for ethane and ethylene/air flames (cf. $S'_{L\infty}$ and $S_{L\infty}$ in Table 1), perhaps because the mass diffusivities of these fuels are closest to those of oxygen of all the fuels considered.

Differences between $S_{L\infty}$ and S_L in Figs. 3 and 4 are significant for the methane and propane/air flames. As will be seen subsequently, methane/air flames are particularly sensitive to preferential-diffusion/stretch interactions and discrepancies in this case can be attributed to stretch. In particular, methane/air flames exhibit nearly neutral behavior at fuel-lean conditions, and rather strong stable behavior at fuel-rich conditions where $S'_{L\infty}$ is significantly lower than $S_{L\infty}$ for outwardly propagating spherical flames (cf. Table 1). Thus, the relatively good agreement of all the methods for methane at fuel-lean conditions while the S_L are appreciably smaller than $S_{L\infty}$ at fuel-rich conditions, seen in Fig. 4, is consistent with this behavior.

A corresponding explanation for the differences between $S_{L\infty}$ and S_L for propane/air flames seen in Fig. 3, however, is problematical even though propane/air flames are relatively responsive to stretch. In particular, propane/air flames are stable for ϕ less than ca. 1.44 so that $S_{L\infty}$ should be greater than S_L for most of the fuel-lean region, rather than the opposite trend seen in Fig. 3. In this case, an available explanation is that the differences are representative of experimental uncertainties with some systematic errors superimposed: the difficulties of prescribing the unburned gas velocity and the value of the stretch, and the uncertainties of finding S_L from derivatives coupled with extrapolation of these results to find $S_{L\infty}$.

A general trend seen in Figs. 3–6 is that the various methods exhibit the greatest discrepancies as limits are approached. This is reasonable because experimental uncertainties are generally largest in regions where the laminar burning velocities become small. Another factor is that both buoyancy-induced strain (which varies with the flow configuration) and the sensitivity of the flames to stretch are largest near limits where S_L is relatively small. Experiments at nonbuoyant conditions, like those of Ronney [34] and references cited therein, as well as careful treatment of effects of finite flame thickness, curvature, unsteadiness, and radiative heat losses, would be required to resolve this difficulty.

Burning Velocity/Stretch Interactions

Given $S_{L\infty}$, plots of $S_{L\infty}/S_L$ as a function of Ka can be constructed as suggested by Eq. 4 for various values of ϕ. The resulting plots from the present measurements of propane, methane, ethane, and ethylene/air flames are illustrated in Figs. 7–10, respectively. The present results for propane/air flames illustrated in Fig. 7 are similar to findings illustrated in Ref. 4 based on the measurements of Refs. 5, 6, and 12, except for a shift of the fuel-equivalence ratios of the results of Ref. 5 analogous

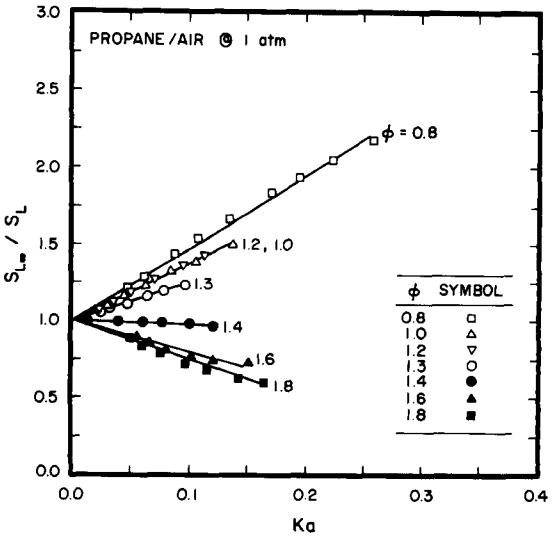

Fig. 7. Laminar burning velocity as a function of Karlovitz number and fuel-equivalence ratio for propane/air mixtures.

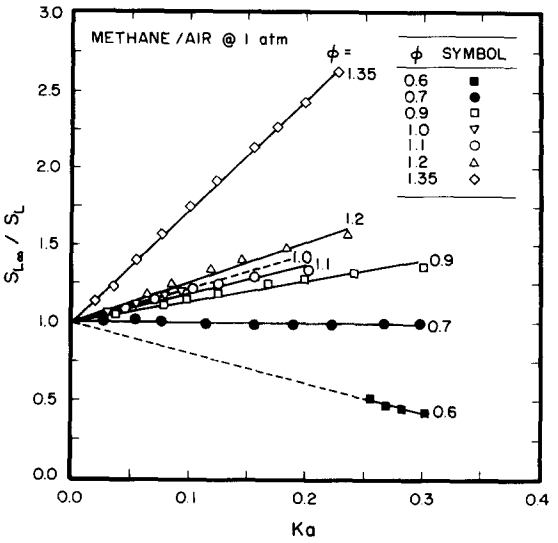

Fig. 8. Laminar burning velocity as a function of Karlovitz number and fuel-equivalence ratio for methane/air mixtures.

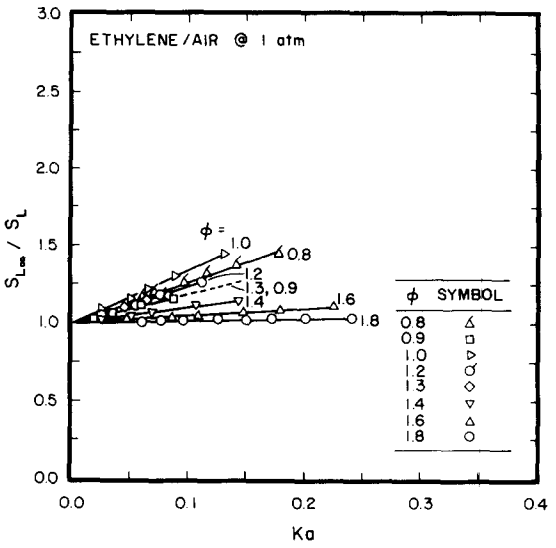

Fig. 10. Laminar burning velocity as a function of Karlovitz number and fuel-equivalence ratio for ethylene/air mixtures.

to the $S_{L\infty}$ of Fig. 3. Additionally, results based on the present analysis of the measurements of Taylor [9] are similar to present results and are not plotted in Figs. 7–10 to avoid cluttering the figures. However, the Taylor [9] results are considered later when Markstein numbers are discussed.

The measurements illustrated in Figs. 7–10 exhibit the linear relationship between $S_{L\infty}/S_L$ and Ka used during the determination of $S_{L\infty}$ as discussed earlier. Thus, the slope of these plots, which is the Markstein number, is clearly independent of Ka over the range of measurements (Ka < 0.30 for present measurements and Ka < 0.36 for results illustrated in Ref. 4). It should be recalled, however, that this range of Ka is not close to extinction conditions where the response of the flames to stretch is likely to change. This behavior implies that the Markstein length scales with the characteristic flame thickness on a local basis, through Eq. 2, which is reasonable because both lengths are representative of distances over which scalar transport is important [10, 11].

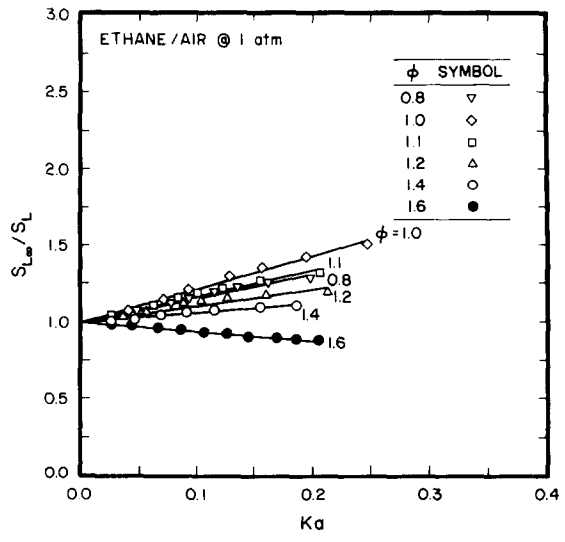

Fig. 9. Laminar burning velocity as a function of Karlovitz number and fuel-equivalence ratio for ethane/air mixtures.

The variation of $S_{L\infty}/S_L$ due to effects of stretch in Figs. 7–10 is substantial, with the following ranges over the present data base: propane, 0.6–2.2 for Ka < 0.25; methane, 0.4–2.7 for Ka < 0.30; ethane, 0.8–1.5 for Ka < 0.25; and ethylene, 1.0–1.5 for Ka < 0.24. Larger variations are probably possible if a larger range of Ka, or conditions nearer flammability limits, had been considered. Such large variations of S_L are reasonable, however, as a result of effects of preferential diffusion induced by stretch. For example, both preferential-diffusion of heat with respect to mass and fuel with respect to oxidant modify flame temperatures, with significant corresponding variations of S_L anticipated due to the rela-

tively large global activation energies of hydrocarbon/air flames [11, 15, 16]. Thus, it is not surprising that effects of stretch on S_L are comparable to effects of varying fuel-equivalence ratios between flammability limits. In view of the strong response of premixed flames to stretch, results such as Figs. 7–10 should provide a good test of detailed chemical kinetic mechanisms used for numerical simulations of premixed laminar flame properties. In particular, stretch effects should provide a strong evaluation of the transport and flow aspects of these simulations because they involve interactions between effects of preferential-diffusion and flow properties.

Hydrodynamic instabilities did not occur within the radius range of present measurements [4, 26]; however, it is of interest to consider effects of preferential-diffusion instability. Neutral and unstable preferential-diffusion conditions can be defined most concisely in terms of Markstein numbers, which are considered subsequently. However, some general trends of preferential-diffusion stability phenomena can be observed from Figs. 7–10 that merit comment. First of all, the methane/air flames are unique among the fuels studied, and perhaps for hydrocarbon/air flames in general, because they are unstable at fuel-lean conditions, similar to $H_2/O_2/N_2$ flames [4], rather than at fuel-rich conditions like the other hydrocarbon/air flames considered during the present study. This can be explained qualitatively using classical phenomenological theories of preferential-diffusion instability [35]. From this argument, the mass flux of the fast-diffusing reactant relative to the slow-diffusing reactant tends to increase at protrusions of the flame surface into the reactants, and tends to decrease at protrusions of the flame surface toward the combustion products. For methane/air mixtures, methane is the fast-diffusing reactant, causing the local fuel-equivalence ratio, and thus the laminar burning velocity, to increase (decrease) for protrusions into the reactants (products) for fuel-lean conditions (see Fig. 4); therefore, the protrusions tend to grow and the flame is unstable [35]. The same considerations for methane/air flames at fuel-rich conditions lead to the conclusion that protrusions are damped and the flame is stable. Similarly, oxygen is the fast-diffusing reactant in propane/air flames, which implies unstable behavior for fuel-rich conditions as observed in Fig. 7. The issue is less clear for ethane and ethylene, which have mass diffusivities intermediate between methane and propane, yielding somewhat reduced response to effects of stretch, as noted earlier, although their unstable regions are observed at fuel-rich conditions like the propane/air flames. In these cases, the preferential diffusion of mass and heat may play a stronger role, although the general nature of preferential-diffusion effects appears to be complex and the specific contribution of preferential diffusion of various species and heat must still be resolved. Additionally, the concepts of the phenomenological theories of preferential diffusion [10, 11, 35] are clearly incomplete because they all imply that transition from stable to unstable preferential-diffusion conditions should occur at fuel-equivalence ratios where maximum laminar burning velocities or flame temperatures are reached (ϕ in the range 1.0–1.2 for present test conditions). Instead, these transitions tend to be shifted toward rich and lean flammability limits for present conditions. The relationship between this behavior and existing theories of effects of stretch on laminar burning velocities is better considered in terms of Markstein numbers, which is discussed next.

Markstein Numbers

The slopes of the plots of $S_{L\infty}/S_L$ as function of Ka yield the Markstein numbers, which are only a function of fuel-equivalence ratio for a given fuel over the existing range of experiments. The resulting values of Ma are summarized in Table 1 and are plotted as a function of ϕ for propane, methane, ethane, and ethylene/air flames in Figs. 11–14, respectively. Results based on the measurements of Palm-Leis and Strehlow [5], Fristrom [6], and Taylor [9] for outwardly propagating spherical flames, analyzed using Eqs. 1–7, are also shown on the plots. The scatter of the data is relatively large, reflecting the uncertainties introduced by finding S_L and Ka from derivatives of r_f as a function of time, and then Ma from another derivative of $S_{L\infty}/S_L$ as a function of Ka. In

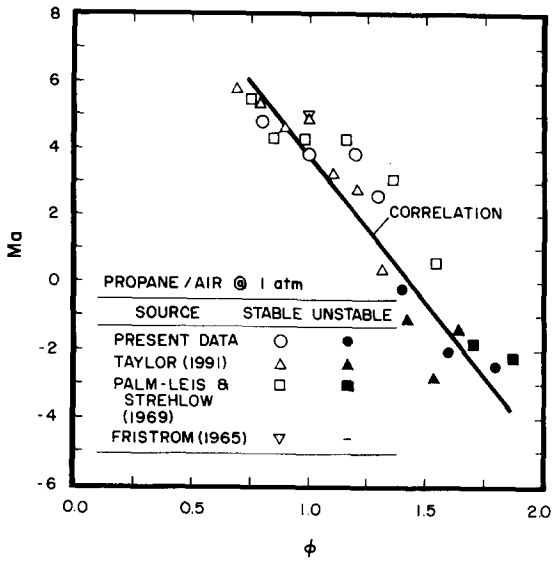

Fig. 11. Markstein number as a function of fuel-equivalence ratio for propane/air mixtures.

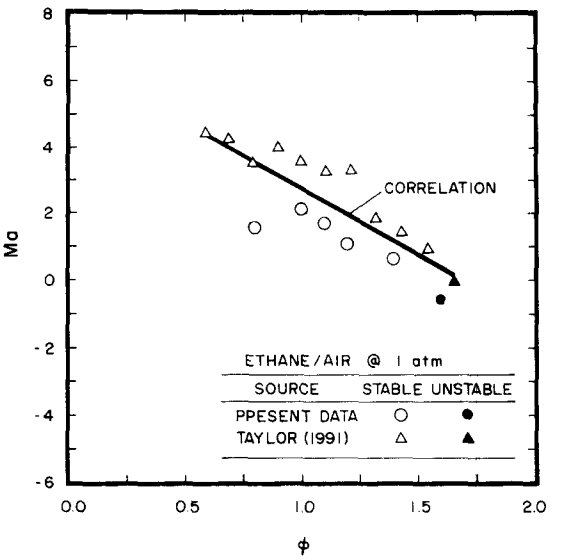

Fig. 13. Markstein number as a function of fuel-equivalence ratio for ethane/air mixtures.

addition, results from Palm-Leis and Strehlow [5] for propane/air mixtures appear to be shifted toward larger fuel-equivalence ratios, similar to the behavior of their measurements of S_{L^∞} illustrated in Fig. 3. Thus, in view of potential problems with the values of ϕ reported in Ref. 5, these results will be excluded from subsequent consideration.

It was of interest to use the measurements illustrated in Figs. 11–14 to help quantify neutral preferential-diffusion conditions and the sensitivity of Ma to variations of ϕ. In general, the variation of Ma with ϕ is expected to be complex, particularly as flammability limits are approached [11]. However, the available ranges of the measurements illustrated in Figs. 11–14 do not closely approach flammability limits and it is difficult to justify more than a linear correlation in view of the scatter of the data.

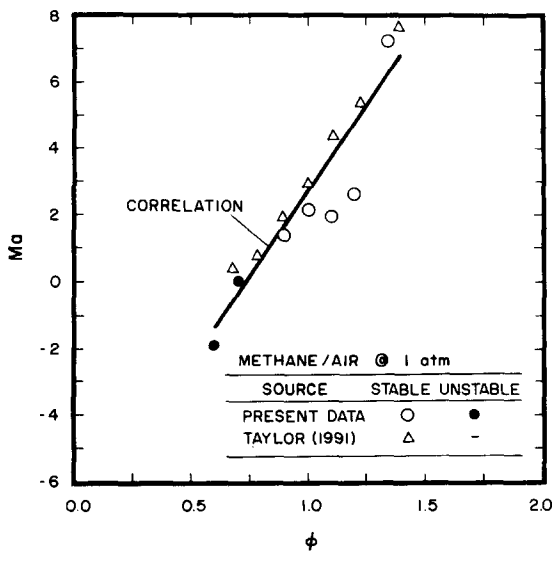

Fig. 12. Markstein number as a function of fuel-equivalence ratio for methane/air mixtures.

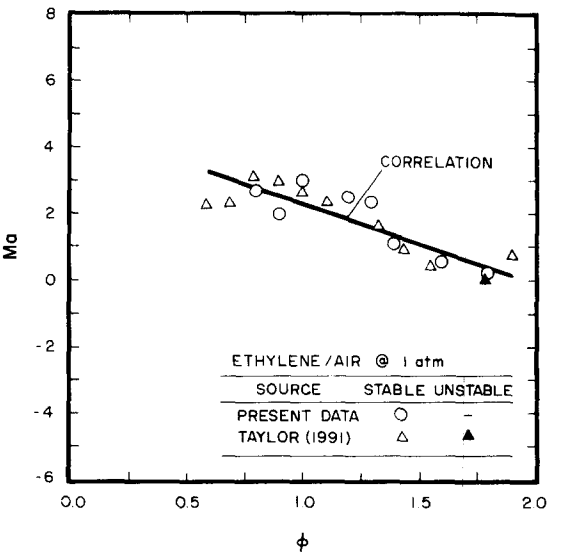

Fig. 14. Markstein number as a function of fuel-equivalence ratio for ethylene/air mixtures.

Thus, the following linear correlation of Ma as a function of ϕ was examined:

$$\mathrm{Ma} = S(\phi - \phi_n). \tag{10}$$

In Eq. 10, ϕ_n is the neutral preferential-diffusion condition where Ma = 0 while S is the sensitivity of Ma to variations of ϕ. The sensitivity S, can have positive or negative values depending on whether the reactant mixture exhibits unstable preferential-diffusion behavior at fuel-equivalence ratios lower or higher than ϕ_n. Least-squares fits using Eq. 10, based on the present measurements and those of Refs. 6 and 9, are also illustrated in Figs. 11–14. The best-fit values of S and ϕ_n, the standard deviations of these quantities, the overall correlation coefficients of the fits, and the ranges of Ka and ϕ of the measurements, are summarized in Table 2. Results in Table 2 also include findings for $H_2/O_2/N_2$ mixtures from Ref. 4, which exhibit a linear relationship between Ma and ϕ over the available range of experiments, as well.

The values of Ma in Figs. 11–14 for hydrocarbon/air mixtures, and summarized in Ref. 4 for $H_2/O_2/N_2$ mixtures, are large, particularly near limits, which implies significant preferential-diffusion/stretch interactions for most practical flames. For example, values of Ma over the available data base are in the range -2.5 to 7.2 for the present hydrocarbon/air flames, and -1.8 to 13.3 for the $H_2/O_2/N_2$ mixtures studied in Ref. 4. The actual range of Ma for given reactants depends on the relative values of S, ϕ_n, and the range of ϕ available due to the presence of rich and lean flammability limits. Thus, methane/air flames have an unusually large S with ϕ_n near the lean flammability limit so that they reach rather large positive values of Ma for fuel-rich conditions where they are stable. On the other hand, $H_2/O_2/N_2$ mixtures have a moderately high value of S, with ϕ_n intermediate between unusually wide flammability limits, so that they can reach both large (in the absolute sense) positive and negative values of Ma. Among the hydrocarbon/air mixtures, propane/air flames are most similar to $H_2/O_2/N_2$ mixtures, having a similar value of ϕ_n, and a larger value of S, so that their maximum absolute values of Ma are only somewhat smaller than the $H_2/O_2/N_2$ mixtures due to narrower flammability limits. Among the flame systems considered in Table 2, the ethane and ethylene/air and the $H_2/O_2/N_2$ mixtures have comparable absolute values of S while the absolute values of S for methane and propane/air flames are somewhat larger. This again highlights the fact that large values of Ma do not necessarily require an unusually large mass diffusivity of one reactant, like hydrogen in the $H_2/O_2/N_2$ flames. On the other hand, the larger absolute values of S for methane and propane/air flames than the other hydrocarbon/air flames seem plausible because their mass diffusivities differ more from that of oxygen than the other hydrocarbons, suggesting greater potential for preferential-diffusion effects. However, preferential-diffusion phenomena are complex and arguments based on relative magnitudes of mass diffusivities fail to explain why the value of S is significantly larger for ethane than

TABLE 2

Summary of Markstein Number Correlations[a]

Reactants	C_3H_8/Air	CH_4/Air	C_2H_6/Air	C_2H_4/Air	$H_2/O_2/N_2$
Slope (S)	−8.8	10.2	−4.0	−2.9	3.9
Intercept (ϕ_n)	1.44	0.74	1.68	1.95	1.50
Maximum Ka	0.25	0.30	0.25	0.24	0.21
ϕ range	0.8–1.8	0.6–1.35	0.8–1.6	0.8–1.8	1.00–4.83
Std. dev. of S	0.8	1.1	0.7	0.4	0.2
Std. dev. of ϕ_n	0.11	0.09	0.22	0.22	0.22
Correl. coef. of Fit	0.95	0.93	0.83	0.86	0.99

[a] Assuming a linear correlation between Ma and ϕ. Hydrocarbon/air results from Taylor [9] and present measurements at 1 atm and 298 ± 3 K. $H_2/O_2/N_2$ results from Kwon et al. [4] at 3 atm and 298 ± 3 K with 12.5%–21.0% O_2 by volume in the O_2/N_2 mixtures.

ethylene/air flames because these two fuels have rather similar mass diffusion properties, cf. Table 1.

In spite of the complexities of preferential-diffusion phenomena, however, some of the general features of present observations do agree with predictions of effects of stretch on premixed laminar flames based on the simplified asymptotic theories discussed by Clavin [11]. These results indicate that scalar transport tends to stabilize flames having modest levels of preferential-diffusion, so that neutral-stability conditions are shifted toward fuel-equivalence ratios on the unstable side of the maximum flame temperature condition. Results in Table 2 generally conform to this trend noting that maximum flame temperatures occur near stoichiometric conditions and that the unstable region is between ϕ_n and the corresponding lean or rich flammability limit for the hydrocarbon/air flames. Thus, the unstable preferential-diffusion regions for the hydrocarbon/air flames, based on the best-fit correlations of Table 2, are as follows: propane, > 1.44; methane, < 0.74; ethane, > 1.68; and ethylene, > 1.95. The $H_2/O_2/N_2$ flames, however, do not agree with theoretical expectations because ϕ_n is shifted toward stable fuel-equivalence ratios in comparison to the maximum flame temperature condition which is near stoichiometric conditions, for example, the unstable region involves $\phi < 1.50$. This type of discrepancy is not unexpected, however, because the fuel-equivalence ratios for maximum flame temperatures and maximum laminar burning velocities are widely separated for $H_2/O_2/N_2$ mixtures—ca. 1.0 and 1.8, respectively [4]—which is not representative of flames satisfying the approximations of the simplified asymptotic theories [11]. This problem should be reduced for the present hydrocarbon/air mixtures where maximum flame temperatures and laminar burning velocities are all in the range 1.0–1.2; thus, the present results should serve as a reasonable basis to evaluate approximate theories in order to gain a better understanding of preferential-diffusion/stretch interactions. Additionally, the large sensitivities of S_L to effects of stretch (Ka), and of Ma to changes of fuel-equivalence ratio and fuel type, should provide a good test of the performance of detailed kinetic simulations of these flames—particularly their treatment of mass transport, heat transport, and flow velocities.

CONCLUSIONS

Effects of positive flame stretch on laminar burning velocities were studied based on measurements for outwardly propagating spherical flames, considering propane, methane, ethane and ethylene/air mixtures with the reactants at normal temperature and pressure. The major conclusions of the study are as follows:

1. Effects of preferential-diffusion/stretch interactions could be correlated according to $S_{L\infty}/S_L = 1 + \mathrm{MaKa}$, where the Markstein number was constant for a particular reactant mixture over the present test range (which involved $\mathrm{Ka} < 0.3$ and did not approach quenching conditions), very similar to earlier observations for $H_2/O_2/N_2$ mixtures [4].
2. Effects of flame stretch on laminar burning velocities were substantial, yielding Markstein numbers in the range -2.5 to 7.2 and corresponding variations of $S_{L\infty}/S_L$ in the range 0.4–2.7—implying significant effects of flame stretch on typical laboratory measurements of laminar burning velocities as well as practical turbulent premixed flames.
3. Markstein numbers varied linearly with fuel-equivalence ratio from the neutral preferential-diffusion condition, according to $\mathrm{Ma} = S(\phi - \phi_n)$, although there was considerable scatter of the data values because Ma determinations involve multiple derivatives of measurements. It should be noted, however, that the available ranges of the measurements do not closely approach flammability limits where the variation of Ma with ϕ might be expected to change [11]. Absolute values of S were in the range 2.9–10.2, being largest and smallest for methane and ethylene/air flames, respectively. Thus, absolute values of Ma tend to increase toward limits, while maximum achievable absolute values involve interactions among S, ϕ_n, and the values of ϕ near the rich and lean flammability limits.

4. Fuel-equivalence ratios for neutral preferential-diffusion conditions were shifted toward the unstable side of the stoichiometric condition, in accord with approximate asymptotic theories [11], yielding the following ranges of ϕ for unstable preferential-diffusion behavior: propane, > 1.44; methane, < 0.74; ethane, > 1.68; and ethylene, > 1.95.
5. The strong sensitivity of laminar premixed flames to preferential-diffusion/stretch interactions, and the rich behavior of these interactions with respect to changes of the reactants and fuel-equivalence ratios, should provide a good test of both approximate and detailed models of premixed flames—particularly their treatment of mass and heat transport phenomena that are central to effects of preferential-diffusion.

This research was supported by the National Science Foundation under Grant No. CTS-9019813. The authors also wish to thank S. Kwon for help with initial development of experimental methods, and the General Motors Research Laboratories, Warren, MI, for donation of the combustion chamber.

REFERENCES

1. Wu, M.-S. Kwon, S., Driscoll, J. F., and Faeth, G. M., *Combust. Sci. Technol.* 78:69–96 (1991).
2. Kwon, S., Wu, M.-S., Driscoll, J. F., and Faeth, G. M., *Combust. Sci. Technol.* 88:221–238 (1992).
3. Kwon, S., and Faeth, G. M., *Twenty-Fourth Symposium (International) on Combustion*, The Combustion Institute, Pittsburgh, 1992, p. 451.
4. Kwon, S., Tseng, L.-K., and Faeth, G. M., *Combust. Flame* 90:230–246 (1992).
5. Palm-Leis, A., and Strehlow, R. A., *Combust. Flame* 13:111–129 (1969).
6. Fristrom, R. M., *Phys. Fluids* 8:273–280 (1965).
7. Dowdy, D. R., Smith, D. B., Taylor, S. C., and Williams, A., *Twenty-Third Symposium (International) on Combustion*, The Combustion Institute, Pittsburgh, 1990, p. 325.
8. Smith, D. B., Taylor, S. C., and Williams. A., personal communication, 1992.
9. Taylor, S. C., Ph.D. thesis, University of Leeds, Leeds, 1991.
10. Markstein, G. H., *Non-Steady Flame Propagation*, Pergamon, New York, 1964, p. 22.
11. Clavin, P., *Prog. Ener. Combust. Sci.* 11:1–59 (1985).
12. Deshaies, B., and Cambray, P., *Combust. Flame* 82:361–375 (1990).
13. Law, C.-K., Zhu, D. L., and Yu, G., *Twenty-First Symposium (International) on Combustion*, The Combustion Institute, Pittsburgh, 1986, p. 1419.
14. Searby, G., and Quinard, J., *Combust. Flame* 82:298–311 (1990).
15. Law, C.-K., *Twenty-Second Symposium (International) on Combustion*, The Combustion Institute, Pittsburgh, 1988, p. 1381.
16. Peters, N., *Twenty-Second Symposium (International) on Combustion*, The Combustion Institute, Pittsburgh, 1988, p. 1231.
17. Strehlow, R. A., and Savage, L. D., *Combust. Flame* 31:209–211 (1978).
18. Yamaoka, I., and Tsuji, H., *Twentieth Symposium (International) on Combustion*, The Combustion Institute, Pittsburgh, 1984, p. 1883.
19. Scholte, T. G., and Vaags, P. B., *Combust. Flame* 3:495–501 (1959).
20. Anderson, J. W., and Fein, R. S., *J. Chem. Phys.* 17:1268–1273 (1949).
21. Gray, K. L., Linnett, J. W., and Mellish, C. E., *Trans. Farad. Soc.* 48:115 (1952).
22. Harris, M. E., Grumer, J., von Elbe, G., and Lewis, B., *Third Symposium on Combustion, Flame and Explosion Phenomena*, Williams & Wilkins. Baltimore, 1949, p. 80.
23. Egerton, A., and Thabet, S. K., *Proc. R. Soc. Lond. A* 211:445–471 (1952).
24. Badami, G. N., and Egerton, H., *Proc. R. Soc. Lond. A* 228:297–332 (1955).
25. Andrews, G. E., and Bradley, D., *Combust. Flame* 19:275–288 (1972).
26. Groff, E. G., *Combust. Flame* 48:51–62 (1982).
27. Lewis, B., and von Elbe, G., *Combustion, Flames and Explosions of Gases*, 2nd ed., Academic, New York, 1961, p. 381.
28. Frankel, M. L., and Sivashinsky, G. I., *Combust. Sci. Technol.* 31:131–138 (1983).
29. Ronney, P. D., and Sivashinsky, G. I., *SIAM J. Appl. Math.* 49:1029–1046 (1989).
30. Matalon, M., and Erneux, T., *SIAM J. Appl. Math.* 44:734–744 (1984).
31. Siegel, R., and Howell, J. R., *Thermal Radiation Heat Transfer*, 2nd ed., McGraw-Hill, New York, 1981, p. 579.
32. Gordon, S., and McBride, B. J., NASA Report SP-273, Washington, 1971.
33. Reid, R. C., Prausnitz, J. M., and Sherwood, T. K., *The Properties of Gases and Liquids*, 3rd ed., McGraw-Hill, New York, 1977, p. 391.
34. Ronney, P. D., *Combust. Flame* 82:1–14 (1990).
35. Manton, J., von Elbe, G., and Lewis, B., *J. Chem. Phys.* 20:153–157 (1952).

Received 2 October 1992; revised 26 August 1993